AFRL-ML-WP-TP-2006-490

A NEW PARADIGM OF FATIGUE VARIABILITY BEHAVIOR AND IMPLICATIONS FOR LIFE PREDICTION (PREPRINT)

S.K. Jha, M.J. Caton, and J.M. Larsen

JUNE 2006

Approved for public release; distribution is unlimited.

STINFO COPY

The U.S. Government is joint author of this work and has the right to use, modify, reproduce, release, perform, display, or disclose the work.

MATERIALS AND MANUFACTURING DIRECTORATE
AIR FORCE RESEARCH LABORATORY
AIR FORCE MATERIEL COMMAND
WRIGHT-PATTERSON AIR FORCE BASE, OH 45433-7750

REPORT DOCUMENTATION PAGE

Form Approved
OMB No. 0704-0188

The public reporting burden for this collection of information is estimated to average 1 hour per response, including the time for reviewing instructions, searching existing data sources, searching existing data sources, gathering and maintaining the data needed, and completing and reviewing the collection of information. Send comments regarding this burden estimate or any other aspect of this collection of information, including suggestions for reducing this burden, to Department of Defense, Washington Headquarters Services, Directorate for Information Operations and Reports (0704-0188), 1215 Jefferson Davis Highway, Suite 1204, Arlington, VA 22202-4302. Respondents should be aware that notwithstanding any other provision of law, no person shall be subject to any penalty for failing to comply with a collection of information if it does not display a currently valid OMB control number. **PLEASE DO NOT RETURN YOUR FORM TO THE ABOVE ADDRESS**.

1. REPORT DATE *(DD-MM-YY)*	2. REPORT TYPE	3. DATES COVERED *(From - To)*
June 2006	Journal Article Preprint	

4. TITLE AND SUBTITLE
A NEW PARADIGM OF FATIGUE VARIABILITY BEHAVIOR AND IMPLICATIONS FOR LIFE PREDICTION (PREPRINT)

5a. CONTRACT NUMBER
In-house

5b. GRANT NUMBER

5c. PROGRAM ELEMENT NUMBER
N/A

6. AUTHOR(S)
S.K. Jha (Universal Technologies Corporation)
M.J. Caton and J.M. Larsen (AFRL/MLLMN)

5d. PROJECT NUMBER
M02R

5e. TASK NUMBER
30

5f. WORK UNIT NUMBER
00

7. PERFORMING ORGANIZATION NAME(S) AND ADDRESS(ES)

Universal Technologies Corporation
Dayton, OH 45432

Metals Branch (AFRL/MLLMN)
Metals, Ceramics and NDE Division
Materials and Manufacturing Directorate
Air Force Research Laboratory, Air Force Materiel Command
Wright-Patterson AFB, OH 45433-7750

8. PERFORMING ORGANIZATION REPORT NUMBER
AFRL-ML-WP-TP-2006-490

9. SPONSORING/MONITORING AGENCY NAME(S) AND ADDRESS(ES)
Materials and Manufacturing Directorate
Air Force Research Laboratory
Air Force Materiel Command
Wright-Patterson AFB, OH 45433-7750

10. SPONSORING/MONITORING AGENCY ACRONYM(S)
AFRL-ML-WP

11. SPONSORING/MONITORING AGENCY REPORT NUMBER(S)
AFRL-ML-WP-TP-2006-490

12. DISTRIBUTION/AVAILABILITY STATEMENT
Approved for public release; distribution is unlimited.

13. SUPPLEMENTARY NOTES
Journal article submitted to Materials Science and Engineering A, published by Elsevier B.V.

The U.S. Government is joint author of this work and has the right to use, modify, reproduce, release, perform, display, or disclose the work. This paper contains color. PAO Case Number: AFRL/WS 06-1240; date cleared: 10 May 2006.

14. ABSTRACT
The treatment of the fatigue variability behavior has traditionally been based on the understanding of the mean-lifetime behavior. With reference to two turbine engine materials, an α+β titanium alloy and a nickel-based superalloy, it is shown that the traditional approach may not accurately describe the fatigue variability behavior of these materials. Decreases in stress level, or microstructural change directed at increasing the mean lifetime, were found to affect mean and worst-case (life-limiting) fatigue behavior differently, and these differences could not be accounted for in the traditional understanding. A new paradigm of fatigue variability was therefore suggested, in which the total uncertainty in lifetime breaks down into the variability in (1) the worst-case mechanism and that in (2) the classical, mean-lifetime governing response. The effects of microstructure and temperature on the fatigue variability behavior were studied with respect to the new paradigm and found to have a very systematic effect on the worst-case and the mean behavior, depending on the degree of influence of these variables on the crack initiation and the growth regime.

15. SUBJECT TERMS
Fatigue variability, α+β titanium alloy, nickel-base superalloy, life-limiting behavior, microstructure, probability of failure

16. SECURITY CLASSIFICATION OF:			17. LIMITATION OF ABSTRACT:	18. NUMBER OF PAGES	19a. NAME OF RESPONSIBLE PERSON (Monitor)
a. REPORT	b. ABSTRACT	c. THIS PAGE			James M. Larsen
Unclassified	Unclassified	Unclassified	SAR	28	19b. TELEPHONE NUMBER *(Include Area Code)* N/A

Standard Form 298 (Rev. 8-98)
Prescribed by ANSI Std. Z39-18

A NEW PARADIGM OF FATIGUE VARIABILITY BEHAVIOR AND IMPLICATIONS FOR LIFE PREDICTION

S. K. Jha[1*], M. J. Caton, and J. M. Larsen

US Air Force Research Laboratory, Wright-Patterson AFB, OH 45431, USA
[1]Universal Technology Corporation, Dayton, OH 45432, USA

ABSTRACT

The treatment of the fatigue variability behavior has traditionally been based on the understanding of the mean-lifetime behavior. With reference to two turbine engine materials, an α+β titanium alloy and a nickel-based superalloy, it is shown that the traditional approach may not accurately describe the fatigue variability behavior of these materials. Decreases in stress level, or microstructural change directed at increasing the mean lifetime, were found to affect mean and worst-case (life-limiting) fatigue behavior differently, and these differences could not be accounted for in the traditional understanding. A new paradigm of fatigue variability was therefore suggested, in which the total uncertainty in lifetime breaks down into the variability in (1) the worst-case mechanism and that in (2) the classical, mean-lifetime governing response. The effects of microstructure and temperature on the fatigue variability behavior were studied with respect to the new paradigm and found to have a very systematic effect on the worst-case and the mean behavior, depending on the degree of influence of these variables on the crack initiation and the growth regime.

Keywords: Fatigue variability, α+β titanium alloy, nickel-base superalloy, life-limiting behavior, microstructure, probability of failure

1. INTRODUCTION

Fatigue lifetime variability behavior is generally described in terms of variability about the overall mean behavior [1-3]. The life prediction approach of fracture critical turbine engine components has also been governed by the conventional understanding of fatigue variability [4,5]. The minimum book life, or the limiting-lifetime, is taken as the extrapolation of the variability about the overall mean behavior corresponding to a predetermined probability of failure (POF), typically taken as 1 in 1000 [4]. As a result, there is large degree of uncertainty associated with the limiting-lifetime prediction and it is estimated that a significant number of components may be discarded while still possessing a considerable fraction of their useful life [5]. A more accurate predicted life may require a re-evaluation of the traditional approach to fatigue variability, especially with respect to its applicability to life prediction.

In this paper, the fatigue variability behavior of two common turbine engine materials is discussed. These were: the $\alpha+\beta$ titanium alloy, Ti-6Al-2Sn-4Zr-6Mo (Ti-6-2-4-6) and a powder metallurgy (P/M) processed nickel-based superalloy. There are few studies of fatigue variability of titanium alloys, although their mean fatigue behavior has been widely studied, and correlations between microstructure and loading variables vs. the mean behavior have been established in many cases [6-9]. In $\alpha+\beta$ titanium alloys, depending on the microstructure, the mean lifetime has been related to the equiaxed α size, and lamellar α/β colony size [7-9]. Decreasing the controlling microstructural unit is known to increase the mean lifetime [9], especially at lower stress levels. It is also well known in titanium alloys that, crack initiation has increased contribution to the total lifetime as the stress level is decreased [10,11]. The relationship of these variables to the fatigue lifetime-variability, however, has not been widely addressed.

The fatigue behavior of P/M nickel-based superalloys has also been reported in many studies [3, 12-18]. These materials are known to fail from crystallographic crack initiation [17,18], as well as processing related constituent particles [17-20] and voids [12,13,15,16]. The treatment of fatigue variability behavior of these materials has been largely focused at obtaining the lifetime distribution from variation in the given microstructural feature as well as, in some cases, the variation in the crack initiation and crack growth rates about the mean response [3, 14-16]. From a design-life perspective, a more important problem may be the competition between mechanisms and their ranking in terms of likelihood of occurrence, as addressed in some studies [21, 22].

Recently, it was shown that, the competition between mechanisms, and the interplay between the number density of relevant microstructural features and the specimen volume, can produce a duality in the S-N fatigue behavior [23]. In a different material [24], the competition, and the sequence of occurrence of mechanisms, was shown to produce a superposition of variability in two mechanisms at the same stress level. These and other studies [25] point to growing evidence that the fatigue variability behavior may not follow the same trend as the mean response. It is crucial to capture and incorporate these fatigue variability responses for reliable life prediction, as it appears this behavior cannot be accounted for in the traditional, mean-based framework.

2. MATERIALS AND EXPERIMENTAL PROCEDURE

The materials in this study were an $\alpha+\beta$ titanium alloy, Ti-6-2-4-6 and a P/M processed nickel-based superalloy. Two heats of the Ti-6-2-4-6 alloy with constant composition but different optical microstructures were considered. These were designated as the pancake and the

disk microstructure and are shown in Fig. 1 (a) and (b), respectively. As shown, both microstructures had a duplex structure with equiaxed primary α (α_p) grains in a transformed β matrix. These however, differed significantly in terms of their crystallographic texture as shown in Fig. 2.

The microstructure of the nickel-based superalloy is shown in Fig. 3. The γ - primary γ' structure is revealed in Fig. 3(a) and the secondary γ' morphology is shown in Fig. 3(b). Since the tertiary γ' precipitates were very fine, they are not resolved at this magnification. The median γ grain size was about 4 μm.

Fatigue specimens were electro-discharge machined in the circumferential orientation from the forgings of the two heats of the titanium alloy. The final machining step involved low stress grinding. Subsequently, each specimen was electropolished (to remove approximately 50 μm from the surface) to eliminate the surface residual stress and to produce a uniform surface condition. Specimens had round-bar geometry with a uniform gage length of about 12.5 mm and a diameter of about 4 mm. The superalloy specimens were also extracted in the circumferential orientation from a pancake forging of the material. For the elevated temperature experiments, a cylindrical, button-head specimen geometry similar to the one described in [26] was used. The gage length was about 15.2 mm and the diameter was about 5 mm.

The fatigue tests were conducted using an MTS 810 servo hydraulic test system equipped with a 458 controller. The experiments were performed in load-control and in lab air. The Ti-6-2-4-6 experiments were performed at room temperature and 260ºC. The temperature of 650 ºC was employed for the superalloy. The stress ratio was 0.05 for all tests, and the frequencies were 20 Hz for the titanium alloy and 0.333 Hz for the superalloy. A resistance-heated furnace with dual zone temperature control was used for the high temperature tests, and control thermocouples

were welded to two locations near the gage of the sample so that the temperature was maintained within ± 2ºC of the set point. A high temperature extensometer was used to record the stress – strain behavior throughout the tests.

Small-crack growth was monitored using the acetate replication technique. Cracks initiating from starter notches, as well as those naturally initiating, were studied. Starter notches were machined using the Femtosecond laser at the University of Michigan, the details of which can be found elsewhere [27]. Additionally, in some samples, notches were machined using a Focused Ion Beam (FIB). Replicas were recorded at predetermined cycle intervals at the static load of 60% of the maximum load in a cycle.

Fractography and orientation imaging microscopy (OIM) were performed in a Cambridge S360FE scanning electron microscope. The microscope was equipped with a TSL OIM system. For imaging, the accelerating voltage of 15 kV, and the probe current of 100 pA was used. For OIM, the accelerating voltage and the probe current of 20 kV and 10 nA were employed. The sample was tilted at 70º with respect to the horizontal axis for OIM, and the working distance was 25 mm. The sample was moved in steps in automated stage control to scan a large area in a single session.

3. FATIGUE VARIABILITY BEHAVIOR OF THE α+β TITANIUM ALLOY

3.1 Mean vs. the Life-Limiting Behavior

The fatigue variability behavior of the Ti-6-2-4-6 pancake microstructure at 25ºC is shown in Fig. 4 (a). The mean-lifetime behavior is also superimposed in the plot. Clearly, the mean behavior followed the classical response to the decrease in stress level, which is attributed to the increasing contribution of the crack initiation regime to the total lifetime [10,11]. At the

same time, the life-limiting behavior had a different response, being relatively insensitive to change in stress level. The minimum lifetime also remained almost unaffected with respect to σ_{max}, as illustrated in Fig. 4(b). The result of these different responses of the lower-tail behavior and the mean lifetime was that the separation between the minimum and mean lifetimes increased with decreasing σ_{max}, causing an increase in the total lifetime-variability (up to 500 X). This indicates that the mean and the lower-tail behavior may be governed by different mechanisms. Another consequence of this type of response was that the lifetime corresponding to the POF of 0.1% (based on the extrapolation of the total variability) decreased with decreasing stress level except at σ_{max} = 820 MPa. This is also shown in Fig. 4(b). As discussed earlier, these fatigue variability responses cannot be accounted for by the mean-life fatigue based understanding and call for an alternate paradigm of fatigue variability behavior.

The separation of the worst-case mechanism, and the mechanism dominating the mean lifetime with decreasing stress level was more evident when the experimental points were plotted as a Cumulative Distribution Function (CDF). This is shown in Fig. 5. A detailed discussion is provided elsewhere [25]. As shown, at the higher stress level (σ_{max} = 1040 MPa), the CDF agreed well with the data. However at the lower stress levels, experimental points exhibited a step-like shape with respect to the CDF, as illustrated for σ_{max} = 860 MPa in Fig. 5. This suggests that the variability in total fatigue lifetime results from a superposition of a worst-case and a long-life mechanism (designated as Type I and Type II respectively).

3.2 Total Variability vs. Variability within Mechanisms

Small-crack growth experiments with different starting notch sizes were conducted to determine the contributions of crack-size regimes to the total variability. The results are

presented in Fig. 6. As shown, no small-crack effect and almost insignificant variability in crack growth behavior was observed when the starting notch dimension (length x depth) was 20 μm x 25 μm or larger, and these small-crack growth data matched with the long-crack behavior. However, a significant small-crack effect was seen when the crack initiated naturally across an equiaxed α grain of size about 4 μm. The maximum contribution to the total lifetime variability is, therefore, expected to originate from crack initiation and early small crack growth (on the order of < 20 – 30 μm).

Figure 4(a) indicates the increasing contribution of crack initiation to the mean lifetime as the stress level is decreased. However, the Type I lifetimes were up to two orders of magnitude smaller. The limiting small-crack growth curves and the limits on the crack initiation sizes were used deterministically to predict the range in the crack growth lifetimes presented in Fig. 7. This figure clearly shows that the range in the Type I lifetimes was related to small crack growth starting from the equiaxed α size scale. Therefore, it can be suggested that the separate response of the mechanisms with decreasing stress level was caused by the increasing crack initiation lifetime of the Type II failures, while the Type I mechanism was controlled by small-crack growth.

3.3 Simulation of Variability in the Type I mechanism

The lifetimes related to the variability in the crack growth rates and the crack initiation sizes were simulated using the Monte Carlo method. The distributions in the crack initiation size and the small-crack growth parameters m and c are presented in Fig. 8. The parameters, m and c, of the crack growth equation are correlated [16,28] and, therefore, were sampled from their joint probability density using the algorithm described in [28]. Further details of the simulation can be

found elsewhere [29]. The simulated lifetimes at σ_{max} = 860 MPa are shown in Fig. 9. As shown, these lifetimes had the same range of values as the experimental Type I lifetimes. It is to be noted that the Type I failures are taken as those comprising the rising part of the step when the data are plotted in the CDF space (see Fig. 5). The simulated lifetimes are compared to the Type I distribution in Fig. 9 (b) at the σ_{max} of 860 MPa. A reasonable agreement between the two is evident. This shows that the uncertainty in the worst-case mechanism was governed purely by the variability in crack growth lifetime starting from the relevant microstructural size scale.

The statistics of the simulated lifetimes are compared with the experimental Type I failures with respect to the stress level in Fig. 10. As shown, the predicted mean lifetimes were in excellent agreement with the experiment (Fig. 10(a)). The standard deviations of the simulated lifetimes (Fig. 10(b)), although under-predicted, were similar to that of the Type I failures and showed the same increasing trend with decreasing stress level. This under-prediction may be due to the limited small-crack data used as input, therefore, the possible under-estimation of the variability in the crack growth behavior. There was small discrepancy between the simulated and the experimental minimum lifetimes (Fig. 10(c)) at some stress levels, which once again may be related to an under-estimation of the input crack growth variability in the simulation. Inclusion of additional small-crack data is expected to further improve the predictions. These simulations however, confirm the observed behavior that the minimum lifetimes may not vary significantly within the range of stress levels considered (see Fig. 4).

3.4 Effect of Microstructure and Temperature

The fatigue variability behavior of the pancake and the disk microstructure are compared in Fig. 11 (a) and (b) at the σ_{max} levels of 860 and 820 MPa, respectively. As shown, at both

stress levels, microstructure had a strong influence on the Type II mechanism but almost no effect on the Type I failure distribution. This led to a decrease in the mean lifetime of the disk material. Since the variability in the Type I mechanism is controlled by crack growth, and given the similar equiaxed α size in the two cases, the very weak response of the worst-case mechanism to microstructure can be attributed to the very similar crack growth behavior of the two microstructures [30]. Due to the dominance of the crack initiation regime in the Type II mechanism, the shift with microstructure may be related to a decrease in the crack initiation lifetime of the disk microstructure. It is not surprising that the crack initiation regime was significantly more sensitive to microstructure than the crack growth [31].

The effect of temperature on the lifetime variability of the two microstructures is shown in Fig. 12 at σ_{max} = 860 MPa. Clearly, the increase in temperature caused a further shift in the Type II mechanism towards smaller lifetimes, as illustrated. However, the Type I lifetimes were not significantly affected by temperature. This was, once again, due to the similar crack growth behavior of the material between room temperature and 260°C [30].

Figures 11 and 12 show that microstructure and temperature had a very systematic influence on the fatigue variability behavior, depending on the degree of sensitivity of crack initiation and growth regimes to these variables. This caused the mean (biased towards the crack initiation controlled, i.e., Type II, mechanism) and the worst-case behavior (crack growth controlled, Type I) to respond very differently to microstructure and temperature.

3.5 An Alternate Paradigm of Fatigue Variability

The vital understanding that follows from the preceding discussion is that, the mean and the worst-case behavior have separate response to operating variables. Therefore, an attempt to

increase the mean lifetime (for e.g., by microstructure modification, decreasing the stress level, or decreasing the temperature) may not produce the same effect on the life-limiting behavior. In Ti-6-2-4-6, this seems to be related to the crack growth vs. the crack initiation control of the life-limiting and the mean behavior respectively. An alternate paradigm is proposed that accounts for this dual response of fatigue variability. This is illustrated in Fig. 13. The total lifetime-variability is due to superposition of variability in the worst-case mechanism and in the long-life mechanism. Further, the uncertainty in the worst-case mechanism is controlled by the variability in crack growth lifetime from equiaxed α size scale. This paradigm can be implemented in a life prediction approach, shown in Fig. 9(b) for σ_{max} = 860 MPa. As discussed previously, the worst-case and the long-life mechanisms are plotted as separate distributions in this figure. The simulated lifetimes based on the crack growth and the crack initiation size variability is also shown for comparison. Since failure can occur by either one of the mechanisms, life prediction can be based on the variability in the worst-case mechanism, i.e., Type I. As illustrated (Fig. 9(b)), this may significantly reduce the uncertainty associated with the traditional approach to life prediction.

4. FATIGUE VARIABILITY OF THE NICKEL-BASED SUPERALLOY

4.1 Mean vs. the Life-Limiting Behavior

The fatigue variability behavior of the nickel-based superalloy at 0.33 Hz, 650°C, and the stress ratio, R of 0.05 is presented in Fig. 14. As shown, there was a significant increase in the mean lifetime with decreasing σ_{max}, but the worst-case, as well as the minimum lifetimes, did not change appreciably. This was similar to the response of the titanium alloy and indicated that the mean and the lower-tail behavior were governed by different mechanisms, which continued to

diverge with decreasing σ_{max}. The experimental points are plotted in the CDF space in Fig. 14(b). Once again, while the CDF agreed well with data at σ_{max} = 1200 MPa, the agreement broke down at lower stress levels.

Characterization of the failures revealed that the life-limiting distribution was related to failure from surface non-metallic particles. The long-life distribution consisted of the surface-void and the subsurface-non-metallic particle related failures. This is illustrated by Figs. 15 (a) and (b). Unlike the titanium alloy, in this case failure was controlled by the processing related microstructural features. However, the nature of fatigue variability was the same. The separation into the worst-case and the mean-lifetime dominating mechanisms in the superalloy material may be a function of the number density and the size distribution of the relevant microstructural features, and also the surface area vs. the volume of the sample [23]. It is also to be noted that the three competing mechanisms (i.e., failure from (i) surface-non metallic particle, (ii) subsurface non-metallic particle, and (iii) surface-void) are realized, in order of their likelihood to cause failure, in order to produce the observed probabilities of occurrence of each (Fig. 14(a)). For example, depending on the stress level, the subsurface non-metallic particle failure can occur only after all possible conditions for the surface non-metallic particle failure have been exhausted in a given sample although all mechanisms may be operating simultaneously.

4.2 Role of Small and Long Crack Growth in the Life-Limiting Mechanism

In order to determine the contribution of crack growth in the life-limiting mechanism, variability in the small crack-growth behavior of naturally initiated cracks was measured and compared to the long-crack behavior obtained from C-T samples. This is presented in Fig. 16. As shown, the variability in the long-crack growth regime was not very significant. On the other

hand, a larger degree of variability was seen in the small-crack regime. The limiting small-crack growth curves, along with the observed range of crack initiation sizes of the life-limiting failures, were used to make deterministic estimates of the bounds on the crack growth lifetimes. The limiting crack growth lifetimes, shown in Fig. 17, described the range in the worst-case lifetimes. As in the case of the titanium alloy, this suggests that the life-limiting failures is controlled purely by crack growth from the relevant microstructural feature.

4.3 Distinction and Similarities between the Behaviors of the Two Materials

Although the titanium alloy and the superalloy failed by different mechanisms, the nature of their fatigue variability behavior was very similar and can be described by the proposed paradigm. In both materials, at higher stress levels, fatigue variability could be described by a single-mode CDF. With decreasing stress level, in both materials, a separation between the worst-case mechanism and the conventionally expected mean-dominating behavior was seen. Although speculative at this point, in the titanium alloy this response may be produced by activation of heterogeneous deformation mechanisms as the stress level is decreased [32-34] or when the microstructural modification is aimed at increasing the mean lifetime. In the superalloy, the effect of the heterogeneity in terms of the spatial distribution of processing related features seems to be more active at lower stress levels, causing the separation between the life-limiting and the mean behavior. In both materials, the uncertainty in the lifetimes of the worst-case mechanism can be described by the variability in small-crack growth from the relevant microstructural size scale.

5. CONCLUSIONS

The following primary conclusions can be drawn from this study:

(i) The fatigue variability behavior of the $\alpha+\beta$ titanium alloy and the nickel-based superalloy could not be accurately described by the conventional understanding, i.e., based on the mean behavior.

(ii) An alternate paradigm was proposed in which the mean behavior is dominated by a different mechanism than the one controlling the life-limiting behavior.

(iii) The mean-lifetime and the worst-case behavior responded differently to a change in microstructure and stress level therefore, affecting the total lifetime-variability.

(iv) The life-limiting behavior in both materials was controlled by the variability in crack growth lifetimes starting from the relevant microstructural size scale.

ACKNOWLEDGEMENTS

This work was performed at the Air Force Research Laboratory, Materials and Manufacturing Directorate, Wright-Patterson Air Force Base, OH. The partial financial support of the Defense Advanced Research Project Agency (DARPA) under DARPA orders M978, Q588, P699, and S271 with Dr. Leo Christodoulou as the program manager is gratefully acknowledged. We acknowledge Mr. Phil Buskohl and Ms. Lindsey Selegue for their assistance with the replication-based small-crack growth experiments. We also wish to acknowledge Dr. Amit Shyam, Mr. Chris Szczepansi, Prof. Wayne Jones, and Prof. Tresa Pollock for assistance with the Femtosecond-laser machining.

REFERENCES

[1] E. A. DeBartolo and B. M. Hillberry, *Int. J. Fatigue*, Vol. 23, p. S49, 2001.

[2] R. Tryon and A. Dey, *J. Aerospace Engng*., Oct 2001, p. 120, 2001.

[3] A. de Bussac and J. C. Lautridou, *Fatigue Fract. Engng. Mater. Struct*., Vol. 16, p. 861, 1993.

[4] B. A. Cowles, *Mater. Sci. Engng*., Vol. A103, p. 63, 1988.

[5] L. Christodoulou and J. M. Larsen, *JOM*, Mar 2004, p. 15, 2004.

[6] D. F. Neal and P. A. Blenkinsop, *Acta Metall*., Vol. 24, p. 59, 1976.

[7] J. A. Hall, *Int J. Fatigue*, Vol. 19, p. S23, 1997.

[8] G. Lutjering, *Mater. Sci. Engng.*, Vol. A263, p. 117, 1997.

[9] Y. Mahajan, H. Margolin, *Metall. Trans.*, Vol. 13A, p. 257, 1982.

[10] J. Ruppen, D. Eylon, and A. J. McEvily, *Metall. Trans. A*, Vol. 11A, p. 1072, 1980.

[11] H. Yokoyama, O. Umezawa, K. Nagai, and T. Suzuki, *ISIJ International*, Vol. 37, p. 1237, 1997.

[12] J. M. Hyzak and I. M. Bernstein, *Metall. Trans.* Vol. 13A, p. 33, 1982.

[13] J. M. Hyzak and I. M. Bernstein, *Metall. Trans.* Vol. 13A, p. 45, 1982.

[14] A. Bruckner-Foit, H. Jackels, and U. Quadfasel, *Fatigue Fract. Engng. Mater. Struct.* Vol. 16, p. 891, 1993.

[15] J. Luo and P. Bowen, *Acta Materialia*, Vol. 51, p. 3521, 2003.

[16] J. Luo and P. Bowen, *Acta Materialia*, Vol. 51, p. 3537, 2003.

[17] T. P. Gabb, J. Telesman, P. T. Kantzos, P. J. Bonacuse, and R. L. Barrie, *NASA/TM-2002 211571*, 2002.

[18] T. P. Gabb, P. J. Bonacuse, L. J. Ghosn, J. W. Sweeny, A. Chatterjee, and K. A. Green, *NASA/TM-2000-209418*, 2000.

[19] D. A. Jablonski, *Materials Sci. Engng.* Vol. 48, p. 189, 1981.

[20] E. S. Huron and P. G. Roth, In: *Superalloys 1996*, 1996.

[21] A. de Bussac, *Fatigue Fract. Engng. Mater. Struct*. Vol. 17, p. 1319, 1994.

[22] M. T. Todinov, *Computers and Structures*, Vol. 79, p. 313, 2001.

[23] K. S. Ravi Chandran and S. K. Jha, *Acta Materialia*, Vol. 53, p. 1867, 2005.

[24] S. K. Jha, J. M. Larsen, and A. H. Rosenberger, *Acta Materialia*, Vol. 53, p. 1293, 2005.

[25] S. K. Jha, J. M. Larsen, A. H. Rosenberger, and G. A. Hartman, *Scripta Materialia*, 2003.

[26] M. J. Caton, S. K. Jha, J. M. Larsen, and A. H. Rosenberger, In: *Superalloys 2004*.

[27] A. Shyam, C. J. Torbet, S. K. Jha, J. M. Larsen, M. J. Caton, C. J. Szczepanski, T. M. Pollock, and J. W. Jones, In: *Superalloys 2004*.

[28] C. J. Annis, In: *Probabilistic aspects of life prediction*, ASTM STP 1450, 2004.

[29] S. K. Jha, J. M. Larsen, and A. H. Rosenberger, In: *Fatigue 2006*.

[30] S. K. Jha, J. M. Larsen, and A. H. Rosenberger, to be published.

[31] S. Suresh, *Fatigue of Materials*, Cambridge University Press, 1991.

[32] A. S. Beranger, X. Feaugas, and M. Clavel, *Mater. Sci. Eng.,* Vol. A172, p. 31, 1993.

[33] X. Feaugas and M. Clavel, *Acta Materialia*, Vol. 45, p. 2685, 1997.

[34] D. L. McDowell, K. Gall, M. F. Horstememyer, and J. Fan, *Engng. Fract. Mech.*, Vol. 70, p. 49, 2003.

Figures:

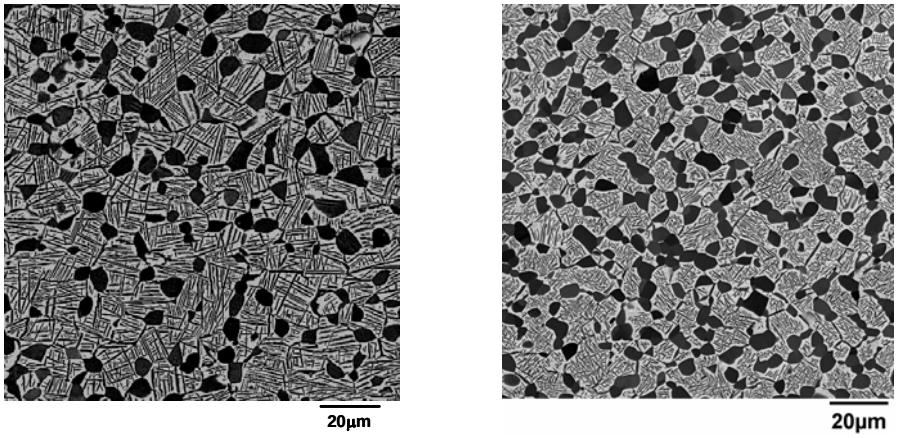

(a) (b)

Fig. 1: Microstructures of the Ti-6-2-4-6 alloy; (a) the pancake microstructure, and (b) the disk microstructure.

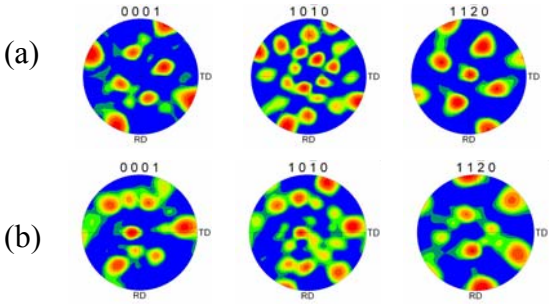

Fig. 2: Crystallographic texture of the two microstructures; (a) pancake and (b) disk.

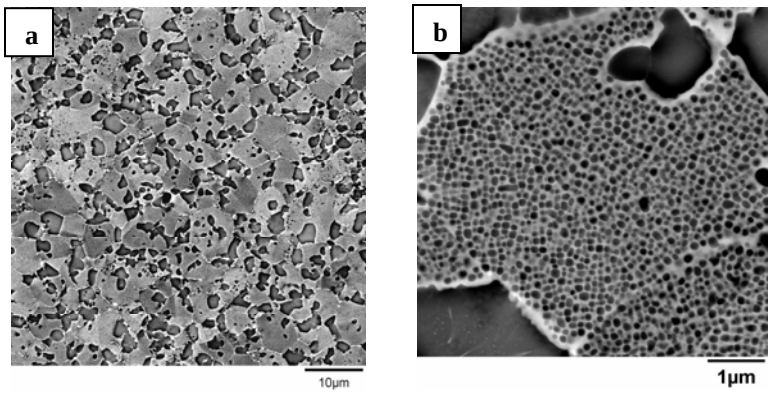

Fig. 3: Microstructure of the nickel-based superalloy; (a) the γ-primary γ' structure, and (b) the secondary γ' structure.

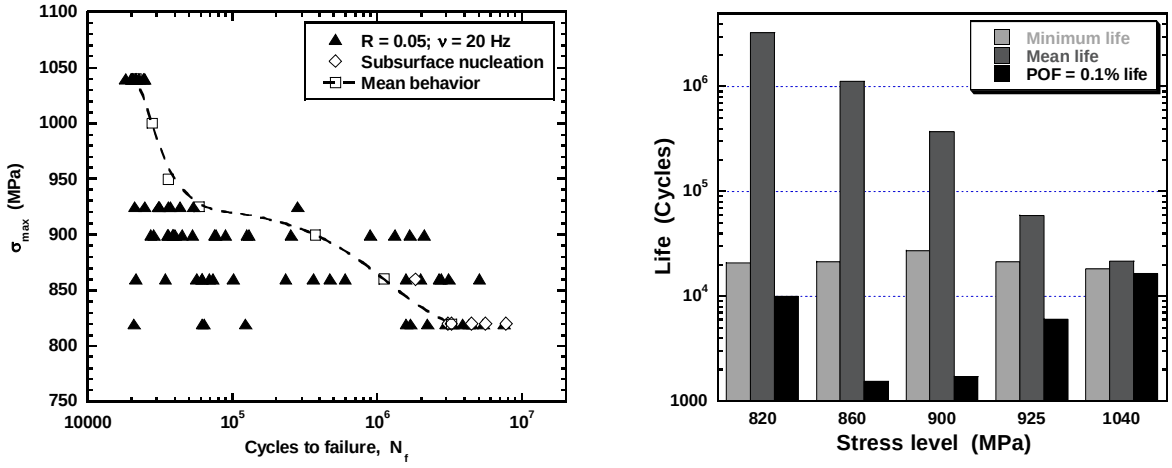

(a) (b)

Fig. 4: Fatigue variability behavior of the Ti-6-2-4-6 alloy at 25°C; (a) mean vs. the life-limiting behavior, and (b) comparison of the B0.1 lifetime with the minimum and the mean lifetime.

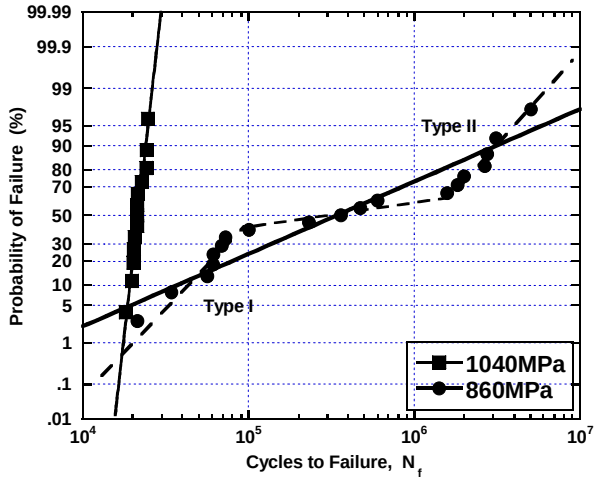

Fig. 5: Experimental points plotted in the CDF space showing the step-like behavior at 860 MPa but a good agreement with the CDF at 1040 MPa.

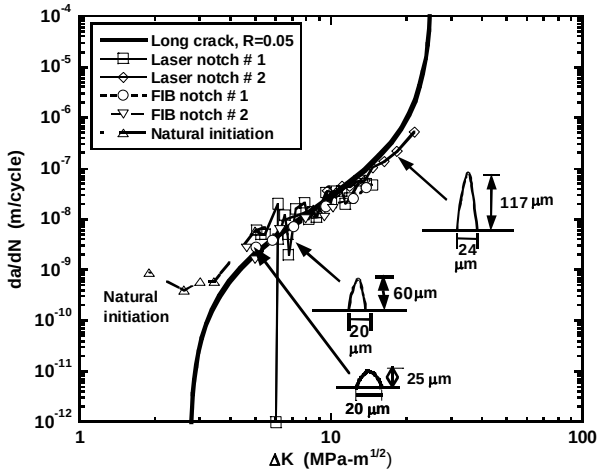

Fig. 6: Small-crack growth behavior from notches and naturally initiated crack in Ti-6-2-4-6.

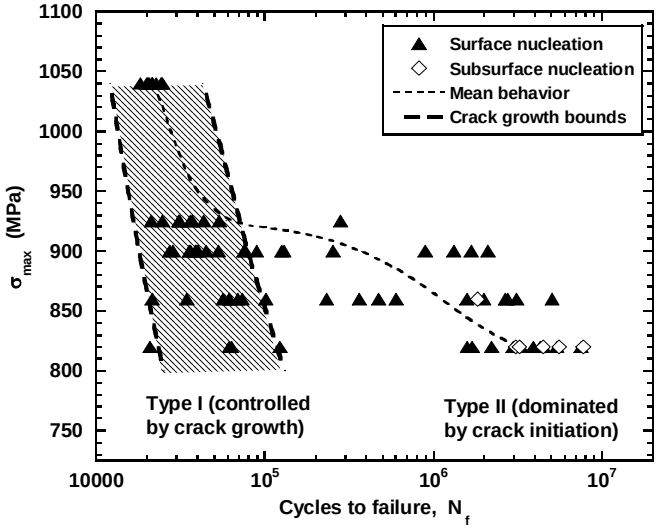

Fig. 7: The deterministic range in crack growth lifetimes based on the limiting small-crack growth curves and the limits on the crack initiation sizes.

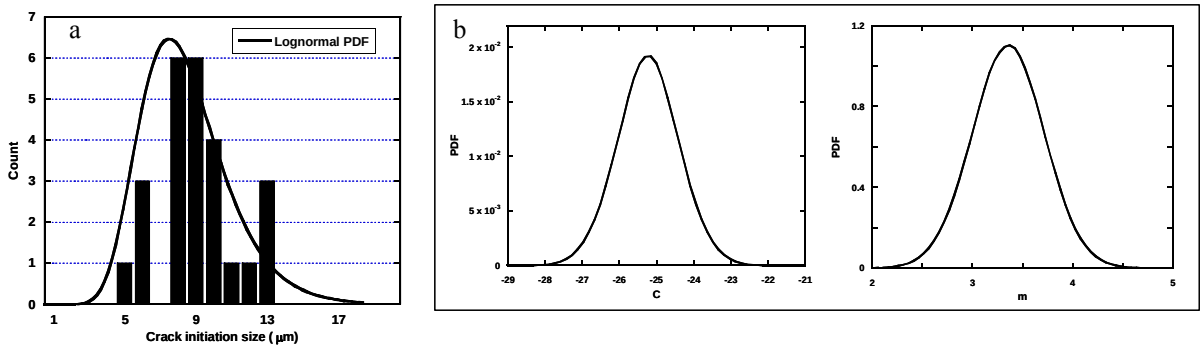

Fig. 8: Inputs to the Monte Carlo Simulation; (a) Crack initiation size distribution, and (b) variability in crack growth behavior.

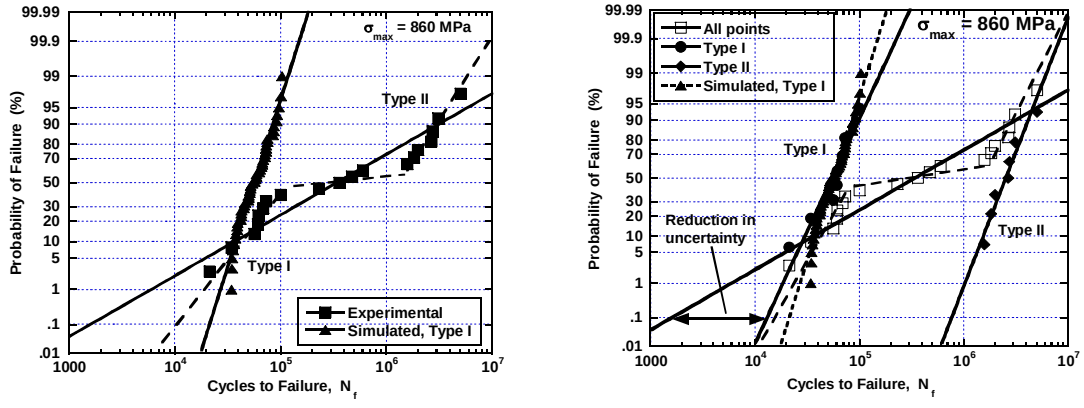

(a) (b)

Fig. 9: Simulated vs. experimental lifetimes; (a) comparison of the simulations with the total lifetime distribution, and (b) comparison of variability in the simulated lifetimes and the experimental Type I distribution.

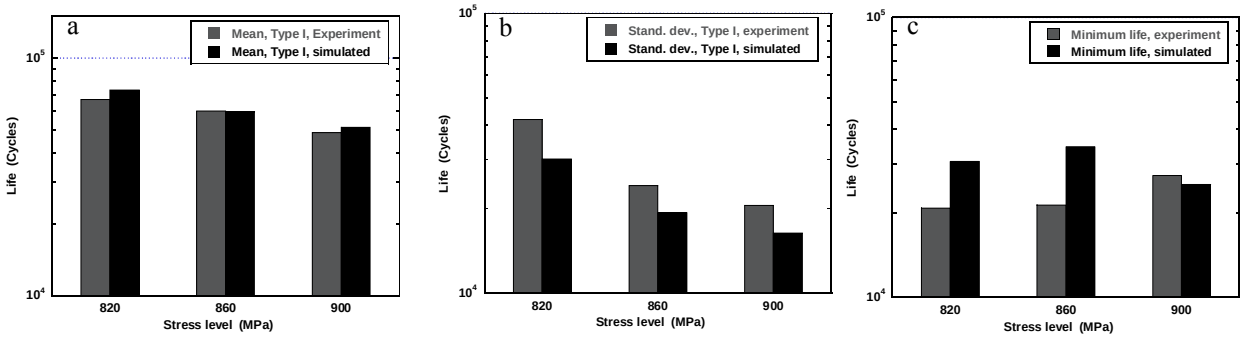

Fig. 10: Comparison of the (a) mean, (b) the standard deviation, and (c) the minimum lifetime of the simulations and experimentally observed Type I failures.

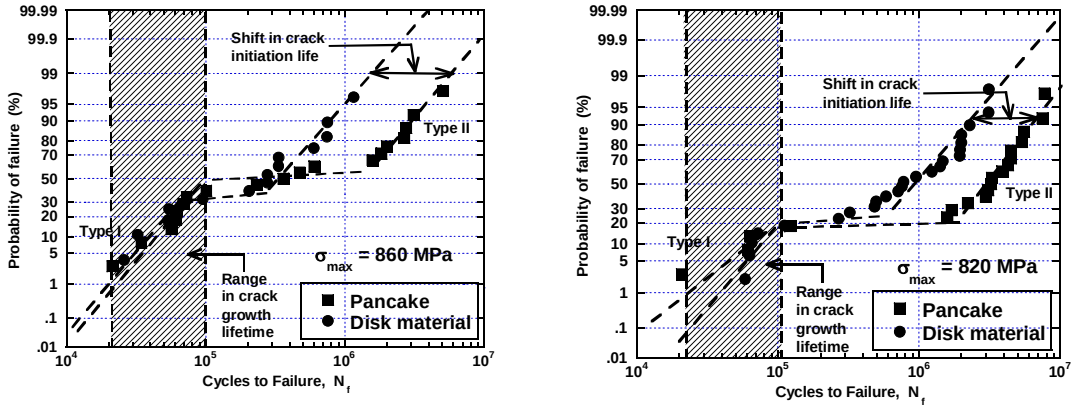

(a) (b)

Fig. 11: Effect of microstructure on the fatigue variability behavior of Ti-6-2-4-6; (a) σ_{max} = 860 MPa, and (b) σ_{max} = 820 MPa.

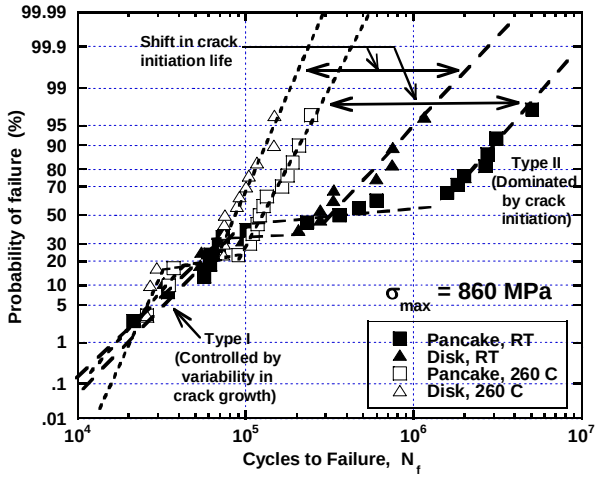

Fig. 12: Effect of temperature on the fatigue variability behavior of Ti-6-2-4-6.

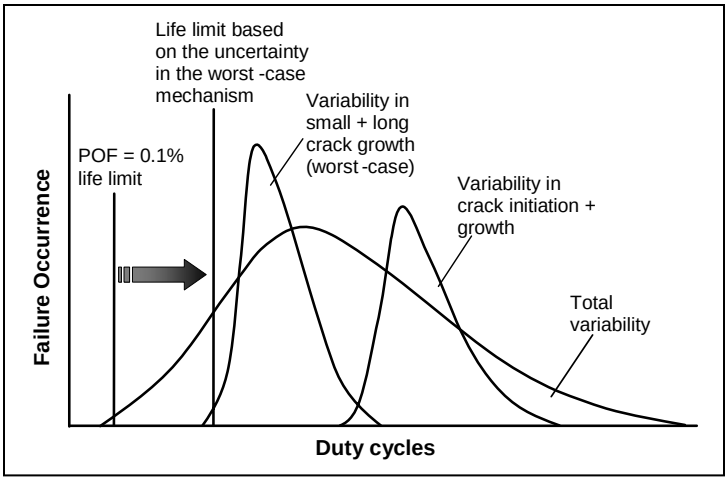

Fig 13: Illustration of the proposed paradigm of fatigue variability behavior.

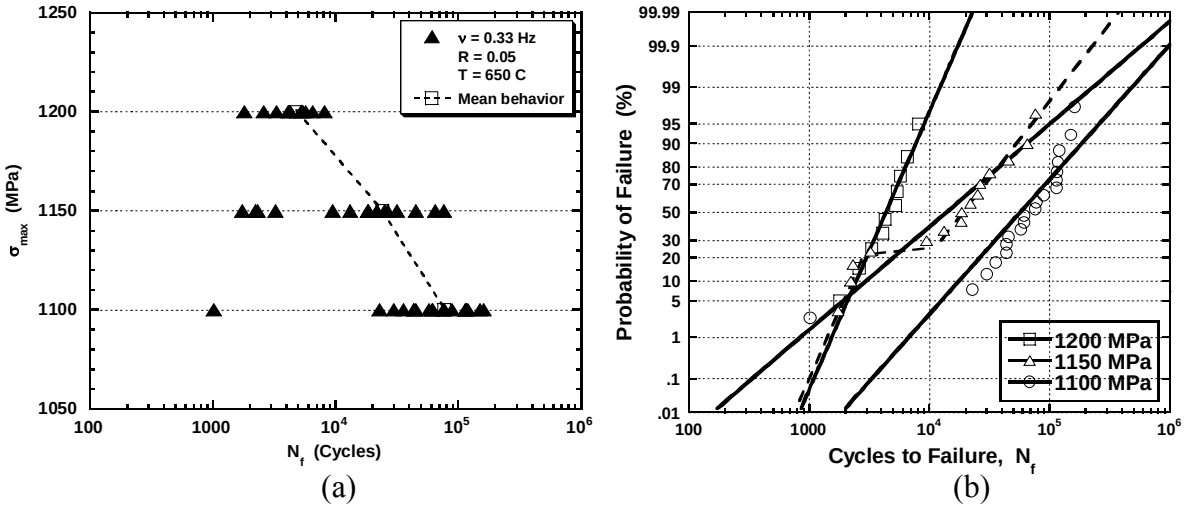

(a) (b)

Fig. 14: Fatigue variability behavior of the nickel-based superalloy at 650°C; (a) Mean vs. the life-limiting behavior, and (b) Experimental points plotted in the CDF space.

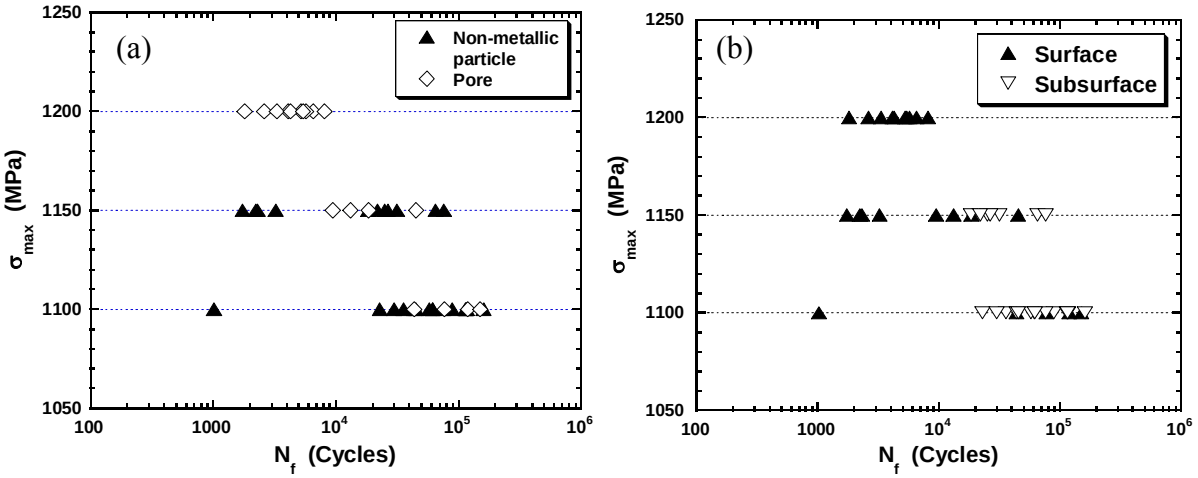

Fig. 15: Competing failure mechanisms in the Ni-based superalloy; (a) Surface vs. subsurface initiated failures, and (b) non-metallic particle vs. void related failures.

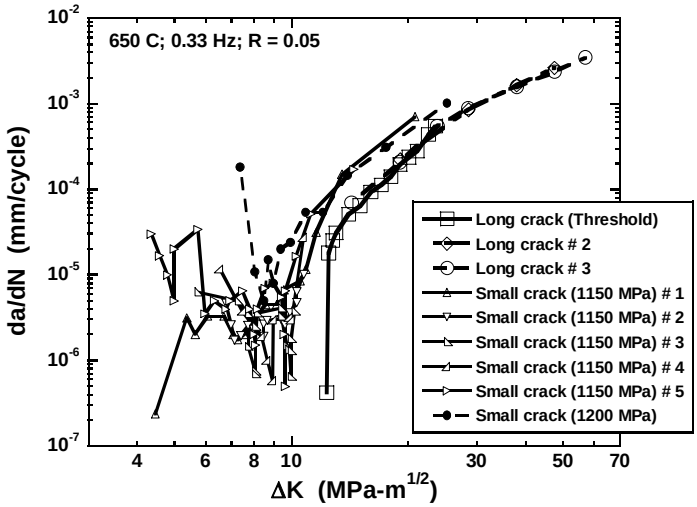

Fig. 16: Variability in the small and the long crack behavior of the nickel-based superalloy.

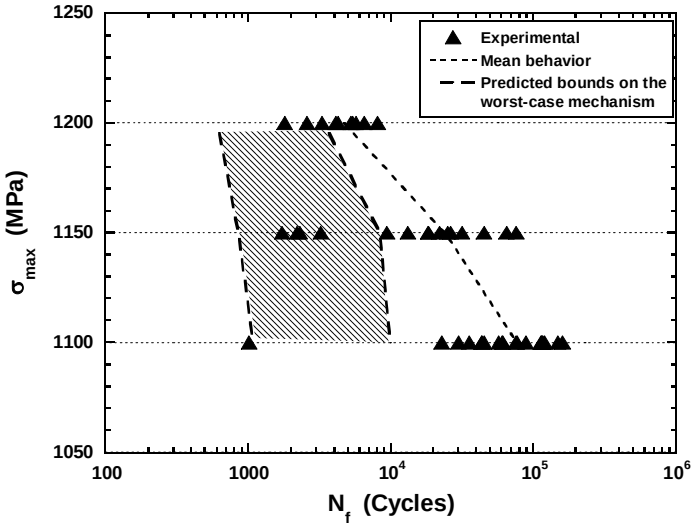

Fig. 17: Deterministic range in the crack growth lifetimes in the superalloy material based on the limiting small crack growth curves and the observed range of crack initiation sizes of the life-limiting mechanism.